PHYSICAL REVIEW B VOLUME 35, NUMBER 4 1 FEBRUARY 1987

Secondary-ion emission from vanadium as a function of incident ion mass and energy in the range 25—275 keV

Patricia G. Blauner and Robert A. Weller
A. W. Wright Nuclear Structure Laboratory, Yale University, New Haven, Connecticut 06511
(Received 28 July 1986)

Measurements of the intensities of low-energy secondary ions emitted from clean and oxidized polycrystalline vanadium surfaces under (25—275)-keV He^+, Ne^+, Ar^+, and Kr^+ bombardment are reported. Whereas the intensities of the metallic-ion species are observed to be proportional to the sputtering yield of vanadium and, therefore, dependent on elastic energy deposition, the intensities of O^+ ions are not. Rather, they increase linearly with increasing projectile velocity in a manner similar to the electronic stopping power or, equivalently, to the yield of secondary electrons. While the production of metallic ions may be described adequately by a number of the proposed models of secondary-ion emission, that of O^+ cannot. The possibility that O^+ is produced by a mechanism similar to electron-stimulated desorption is discussed.

I. INTRODUCTION

Secondary-ion emission is one of the most complex and least understood aspects of sputtering. In the last few years, progress has been made toward unraveling this complicated phenomenon primarily by constructing models which stress the importance of global properties such as the band structure and work function of the bombarded surface (see Refs. 1—5 for reviews of the subject). Recently, however, Yu and associates have argued that for systems which show strong enhancements in ion production in the presence of electronegative elements, a description in terms of the breaking of local chemical bonds is more appropriate.[5] Although the experimental evidence supporting this hypothesis is convincing, several other experiments have indicated that, in a variety of circumstances, another mechanism plays an important role in ion emission from such systems.[6—11] These experiments have concentrated on the emission of positive ions of electronegative elements, since the formation of these ions cannot be explained by the chemical bond-breaking that may accompany the elastic recoil of a struck atom.

The first such results were reported by Williams.[6] In an investigation of secondary-ion emission from fluorinated silicon and chlorinated aluminum targets under (2—10)-keV Ar^+ and $O_2{}^+$ bombardment, he observed unexpectedly strong F^+ and Cl^+ yields. He found that the F^+ signal from the Si sample strongly resembled that of electronically desorbed fluorine. Furthermore, the yield of F^+ was reported to correlate with the Si *LVV* Auger electron signal produced under similar bombardment conditions. He thus concluded that F^+ was being electronically desorbed by silicon *LVV* Auger electrons.

Unexpectedly high yields of electronegative species have also been observed under high energy ion bombardment. In a survey of secondary ion emission from metal targets bombarded by MeV heavy ions, Weller and collaborators have reported unusually large relative yields of several species of positive ions of electronegative target constituents.[7,8] A more detailed study of ion emission from vanadium as a function of bombardment energy in the MeV range showed that while the yield of metal ions has the same beam energy dependence as the predicted sputtering yield of the metal, the yields of O^+ and F^+ do not.[9] A similar difference in primary beam energy dependences in the MeV regime was reported in the work of Becker *et al.*[10] Most recently, Blauner *et al.* have reported secondary ion emission from oxidized V and Al under (25—300)-keV light-ion (H^+,He^+) bombardment which shows characteristics similar to those found using MeV heavy ions.[11]

The studies using high-velocity primary ions are especially interesting since work on secondary ion emission has previously concentrated almost exclusively on low-energy heavy-ion projectiles (typically Ar^+ below 10 keV), where elastic processes are principally responsible for energy deposition in the target. In extending the velocity of the primary ions, it has become clear that mechanisms not addressed by the current models of secondary ion emission can become important or even the dominant channels for the production of low-energy secondary ions.

The goal of the work presented here has been to systematically investigate the role of the projectile mass and energy in secondary-ion production by studying clean and oxidized vanadium surfaces under bombardment by (25—275)-keV ions. By using primary ions ranging from He to Kr, we have been able to investigate systems with widely varying contributions of elastic and inelastic energy deposition. This is illustrated in Fig. 1 which plots estimates of the nuclear (S_n) and electronic (S_e) stopping powers of He and Kr in V. In the energy range under consideration, for the case of Kr bombardment, S_n is greater than S_e, while for He bombardment S_e substantially exceeds S_n. Vanadium targets were chosen for this investigation since previous studies of V under MeV heavy- and keV light-ion bombardment have demonstrated large O^+ yields.[7—9,11] A similar study of clean and oxidized aluminum surfaces will be presented in a subsequent paper.[12]

 ©1987 The American Physical Society

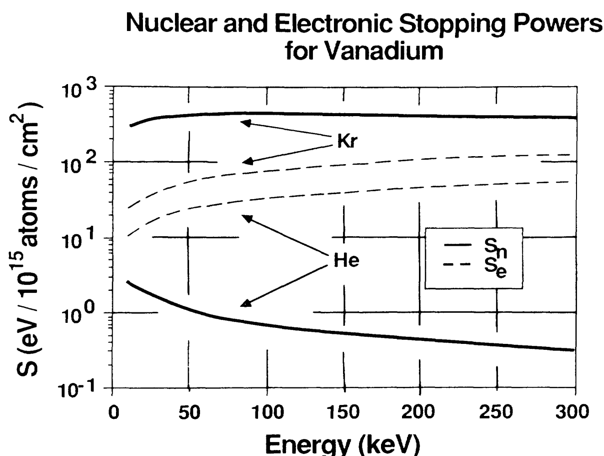

FIG. 1. Comparison of the nuclear S_n and electronic S_e stopping powers of (10—300)-keV He and Kr in a vanadium target. The stopping powers were calculated according to the formalism in Ref. 13. Sputtering yields Y (the mean number of emitted atoms per incident projectile) are predicted to be proportional to S_n (Ref. 24).

II. EXPERIMENTAL

Positive secondary-ion mass spectra were measured from clean and oxidized V targets under (25—275)-keV He^+, Ne^+, Ar^+, and Kr^+ bombardment using the apparatus shown schematically in Fig. 2. Mass analyzed beams from a 300-keV Cockcroft-Walton accelerator were incident on targets located in a UHV scattering chamber. The resulting secondary ions were analyzed by a quadrupole mass spectrometer located at 30° to the beam axis. Through differential pumping, pressures of $<3\times10^{-10}$ Torr were maintained in the scattering chamber when it was open to the accelerator.

The targets used in the study were thick (0.025 mm) cold-rolled polycrystalline V (purity $>99.95\%$) all cut from the same stock. Prior to being introduced into vacuum, they were soaked in warm distilled water and Alconox detergent for 15 min, soaked in warm distilled water for 15 min, degreased in trichlorotrifluoroethane (Freon TF) for 5 min, rinsed in distilled water, soaked in isopropyl alcohol for 15 min, and, lastly, hot air dried. The vacuum chamber was then baked for 1.5 days at approximately 130 °C, resulting in a base pressure of $<2\times10^{-10}$ Torr ($<5\times10^{-10}$ for analysis of oxide surfaces). Clean surfaces were obtained by sputter-etching with 0.5 C/cm^2 of 200-keV Ar^+ rastered over an area of approximately 40 mm^2. This was estimated to remove more than 2000 monolayers of material from the target.[13] The irradiation also resulted in substantial heating of the target. The temperature of the irradiated area was measured with an optical pyrometer to be approximately 875 °C. The absence of foreign material on the surface after this procedure was confirmed both by secondary ion mass analysis and by Auger electron spectroscopy. When required, the target was then oxidized by exposure to 1000 L O_2 (1×10^{-6} Torr for 1000 sec), after which an O_2 pressure of 5×10^{-8} Torr was maintained in the chamber. This, combined with low primary beam current densities, was found to yield reproducible, steady-state secondary-ion emission with no measurable contribution from gas-phase ionization of the residual O_2.

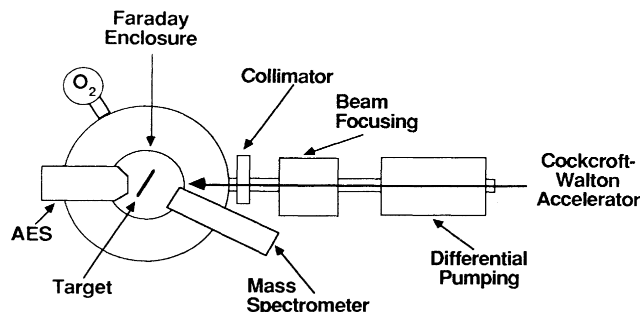

FIG. 2. Arrangement of the apparatus. Primary ions were incident at 30° with respect to the target normal, which was aligned along the spectrometer axis. The Faraday enclosure surrounded the targets except for openings for the primary beam and spectrometer. The Auger electron spectrometer was located opposite the primary beam.

As shown in Fig. 2, the targets were oriented facing the mass spectrometer and were surrounded by a Faraday enclosure to improve beam current integration. Current integrated in this manner was estimated to be accurate to within 20%, with high readings being attributable to secondary electrons not contained within the enclosure. The incident ion beams were collimated so that approximately 3 mm^2 of the target was irradiated. Total beam currents of 0.5—1 nA were used when bombarding the oxidized target in order to minimize damage to the surface and to maintain count rates sufficiently low to operate in pulse counting mode. This was increased to 5—10 nA for the clean target.

Low-energy secondary ions were analyzed using a quadrupole mass spectrometer which has been described in a previous publication.[11] It was programmed to monitor the positive secondary-ion intensities at discrete points in the mass range 1—205 u/e, repeatedly cycling through the ion species of interest on the basis of the integrated beam current measured on the target. The spectrometer's prefilter was adjusted to analyze 5-eV ions with a band pass of 3 eV full width at half maximum.

Data were obtained by the following procedure. The target was first cleaned and oxidized (when appropriate) as described above. Then a series of measurements of secondary-ion mass spectra were made at 25-keV increments with a single primary beam species. Staggered, repeated measurements were made every 50 keV in order to monitor any changes in the spectra due to changes in the target surface or beam dynamics. In order to monitor longer term changes, measurements were taken using a standard 200-keV Ar^+ beam both before and after the measurements made with each beam species. Such variations were observed to be less than $\pm15\%$ over the course of all measurements. Analyses of the clean target under bombardment by a given beam species were made within a 4-h period after sputter-etching the surface. Minimum

changes were observed in the secondary ion intensities over the course of this period. The target was recleaned prior to taking measurements with other bombarding species.

III. RESULTS

The relative intensities of the predominant low-energy positive secondary-ion species measured for each ion beam at 200 keV are shown in Table I. These values represent an average over repeated measurements and hence the uncertainties stated represent the measured reproducibility of the relative ion yields. We stress that no corrections have been made for the transmission of the spectrometer as a function of secondary ion mass, so that sensitivity to species with a mass to charge ratio greater than approximately 40 u/e is increasingly diminished.[14,15]

As Table I indicates, V^+, VO^+, and various oxide clusters are prevalent in the spectra measured from the oxidized surface bombarded by Ne, Ar, and Kr. For all primary ion beams, the intensity of VO^+ is comparable to, but less than that of V^+. In addition, O^+ is a major constituent of the spectra obtained with the lighter primary beams. In the case of He^+ bombardment, the O^+ intensity exceeds that of all other ion species. This is in agreement with previous results obtained under similar conditions using H^+, H_2^+, and He^+ beams.[11]

The spectra obtained from the clean V surface are quite different than those from the oxide targets. These spectra contain significant intensities of only metallic cluster ions, V_n^+ ($n = 1,2,3,\ldots$). As has been reported by several investigators, the yields of these clusters fall off monotonically with increasing n.[16,17] Despite the limited mass transmission of our instrument, we were able to detect clusters up to V_4^+. The yield of V^+ is approximately two orders of magnitude smaller than that measured from the oxidized surface, whereas V_2^+ is comparably larger. The latter observations are in agreement with the spectra reported by Müller and Benninghoven for 3-keV Ar^+ bom-

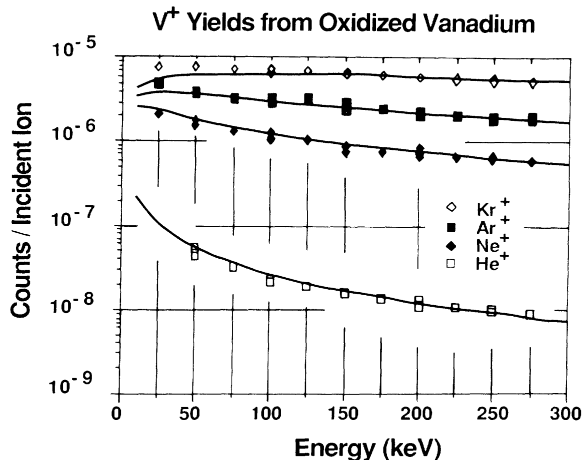

FIG. 3. Intensity of V^+ secondary ions from oxidized V as a function of primary beam (He^+, Ne^+, Ar^+, and Kr^+) energy. The solid curves represent the sputtering yields for pure V, as explained in the text.

TABLE I. Relative intensities ($100\times I_i/\Sigma I_i$, where I_i is the intensity of the ith ion species) of those secondary-ion species emitted from oxidized and clean V surfaces under 200 keV ion bombardment which contribute $\geq 0.1\%$. The measured intensities in counts per incident ion of the V^+ peaks for the various primary ion beams were He, $(1.16\pm0.08)\times10^{-8}$; Ne, $(7.6\pm0.9)\times10^{-7}$ (oxidized) and $(6.8\pm0.5)\times10^{-9}$ (clean); Ar, $(2.2\pm0.1)\times10^{-6}$ (oxidized) and $(1.5\pm0.2)\times10^{-8}$ (clean); Kr, $(5.85\pm0.02)\times10^{-6}$. The values quoted are averages over repeated measurements and hence the uncertainties assigned represent the measured reproducibility of the relative ion yields.

Beam	O^+	V^+	VH^+	VO^+	VOH^+	VO_2^+	VO_2H^+	V_2^+	V_2H^+	V_2O^+	$(VO)_2^+$	V_3^+	V_3H^+	V_4^+	V_4H^+
							Oxidized surface								
He	89 (±1)	5.7 (±0.7)		4.6 (±0.3)	0.5 (±0.2)										
Ne	19.1 (±0.6)	43.4 (±0.9)	0.4 (±0.1)	32 (±2)	4 (±1)	0.4 (±0.1)	0.4 (±0.1)			0.1	0.2				
Ar	5.6 (±0.3)	51.1 (±0.9)	0.4 (±0.1)	38 (±1)	4.0 (±0.2)	0.4 (±0.1)	0.3			0.2	0.3 (±0.1)				
Kr	1.5	54.6 (±0.1)	0.4	34.2 (±0.2)	7.9 (±0.2)	0.4	0.6			0.2	0.3				
								Clean surface							
Ne		32 (±2)	2.4 (±0.6)					22.6 (±0.3)	37 (±2)			2 (±3)	2.8 (±0.6)	0.6 (±0.8)	0.2 (±0.3)
Ar		44 (±4)	1.8 (±0.6)					27 (±3)	20 (±6)			4.4 (±0.1)	1.5 (±0.4)	0.8 (±0.1)	0.3 (±0.1)

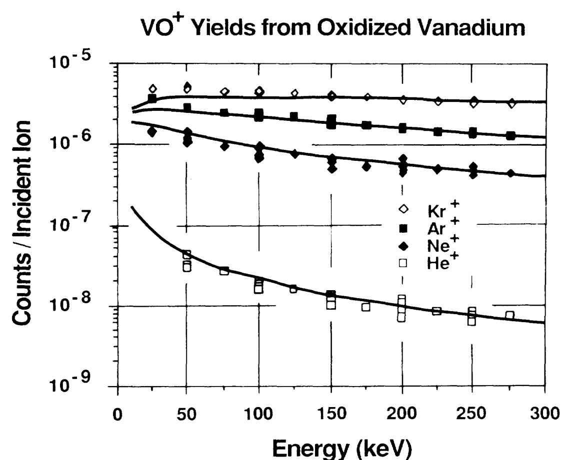

FIG. 4. Intensity of VO^+ secondary ions from oxidized V as a function of primary beam (He^+, Ne^+, Ar^+, and Kr^+) energy. The solid curves represent the sputtering yields for pure V, as explained in the text.

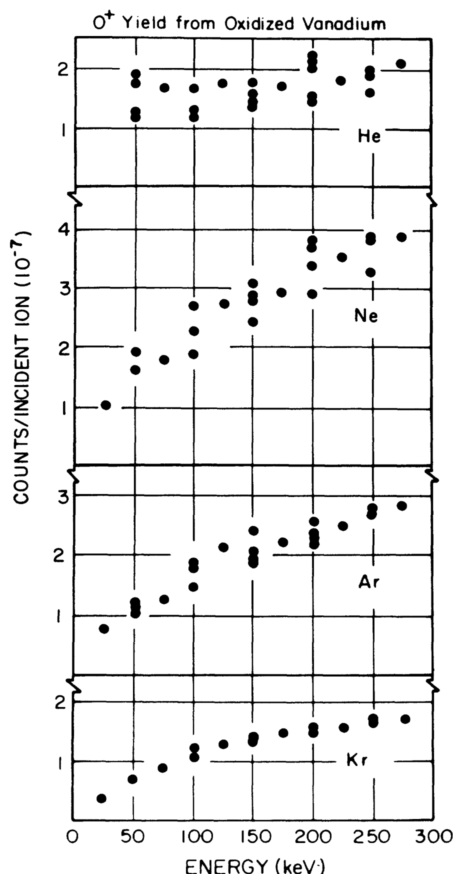

FIG. 5. Intensity of O^+ secondary ions from oxidized V as a function of primary beam (He^+, Ne^+, Ar^+, and Kr^+) energy.

bardment of similarly prepared V surfaces.[17]

Figures 3–6 show, respectively, the primary beam energy dependences of V^+, VO^+, and O^+ from the oxidized target and V^+ and $V_2{}^+$ from the clean target. The scatter present in the data (generally less than $\pm 15\%$) represent variations in the absolute ion intensities. This is far greater than the uncertainties in the relative ion intensities as shown in Table I and is symptomatic of variations in the beam focusing and current integration. The solid curves represent the sputtering yield Y of pure vanadium as calculated by the semiempirical formula of Matsunami *et al.*[13] This has been chosen as a standard for comparison, since the semiempirical formula has not been generalized to multicomponent materials and, in particular, oxides. The curves have been scaled by the fitting constants C_i, which are the ratios of the measured ion intensities to the predicted values of Y at beam energies of 200 keV (Table II). So defined, the C_i represent the combined effect of the ionization probability, the spectrometer acceptance (both angular and energy) and transmission, and the detector efficiency.

Figures 3–6 illustrate a number of important points. As is shown in Figs. 3, 4, and 6, the yields of the low-energy metallic ion species (including oxides and clusters) are approximately proportional to the sputtering yield of pure V over the range of projectile energies E_1 that was measured. Some deviation from this proportionality is, however, evident in the data obtained with the heavier beams near the peak in their sputtering yields. (Such a deviation has also been seen in sputtering yield measure-

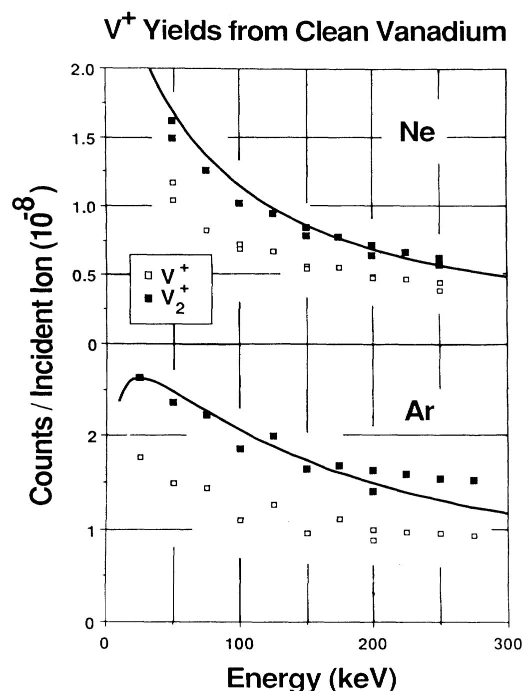

FIG. 6. Intensity of V^+ and $V_2{}^+$ secondary ions from clean V as a function of primary beam (He^+, Ne^+, Ar^+, and Kr^+) energy. The solid curves represent the sputtering yields for pure V, as explained in the text.

TABLE II. Scaling coefficients C_i used to fit the sputtering yield to the data in Figs. 3, 4, and 6: $I_i(E_1,Z_1)=C_iY(E_1,Z_1)$, where I_i is the ion intensity of the ith secondary-ion species measured under 200-keV ion bombardment, E_1 and Z_1 are the energy and atomic number of the primary ion, and Y is the sputtering yield as calculated by the semiempirical formula of Matsunami *et al.* (Ref. 13).

	C_i		
	Oxide surface		Clean surface
Beam	V^+ (10^{-6})	VO^+ (10^{-6})	V^+ (10^{-8})
He^+	4.6	3.7	
Ne^+	2.3	1.7	2.1
Ar^+	1.5	1.1	1.0
Kr^+	1.2	0.75	

ments and is generally attributed to nonlinear effects in the collision cascade which have not been taken into account in the calculations.) In addition, the yields of the metallic ion species remain approximately the same fraction of Y as a function of the atomic species of the projectile, Z_1. An examination of the proportionality constants listed in Table II does show a systematic decrease in C_i between He and Kr. The decrease is, however, small in comparison with the factor of 2000 difference in Y for these two projectiles. It could reflect inaccuracies in the predicted value of Y, a real decrease in the ionization probability with increasing Z_1, or a shifting of the secondary-ion energy distributions as a function of Z_1 (the spectrometer used sampled only a narrow range of secondary-ion energies). The last alternative is least likely since the shape of secondary-ion energy distributions has been shown to be insensitive to Z_1.[1]

In contrast to the metallic species, the intensities of low-energy O^+ vary by less than a factor of 3 over the range of projectiles and increase monotonically as a function of E_1 (Fig. 5). As is shown in Fig. 7, this increase is linear with projectile velocity. Furthermore, for the heavier primary ions (Ne^+, Ar^+, and Kr^+) at a given velocity, the O^+ intensities are identical within the uncertainties of the measurements.

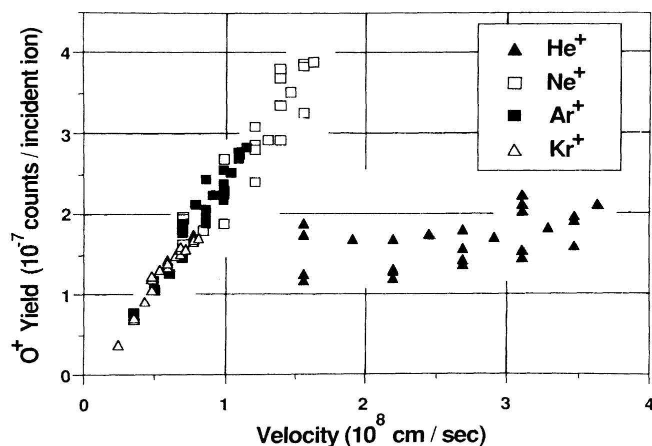

FIG. 7. Intensity of O^+ secondary ions from oxidized V as a function of primary ion (He^+, Ne^+, Ar^+, and Kr^+) velocity.

IV. DISCUSSION

These results may be summarized most concisely by dividing the observed positive secondary ion species into two categories. The first consists of metallic oxide ($M_nO_m{}^+$) and metallic cluster ($M_n{}^+$) ions. The yields of these species are observed to be proportional to the sputtering yield of pure V both as a function of E_1 and Z_1. The second category consists of O^+ alone. The yield of this species is observed to be unrelated to the sputtering yield of the V substrate and, for the projectile energies considered, to increase linearly with projectile velocity. Furthermore, the observed intensities of O^+ are identical for Ne^+, Ar^+, and Kr^+ bombardment at a given velocity.

From these observations, it is clear that the previously reported large relative yields of O^+ observed under MeV heavy and keV light ion bombardment result not only from enhanced O^+ production, but also from a decreased production of positive metallic ions. The latter is consistent with the decrease in the sputtering yield of V under these bombardment conditions. Since production of low-energy metallic ions in all cases has been found to be proportional to the calculated sputtering yield both as a function of E_1 and Z_1, we conclude that these secondary-ion species are ejected from the surface in much the same manner as the neutral sputtered species and that they are ionized by mechanisms which are relatively independent of the properties of the primary projectile. This interpretation is consistent with a number of the proposed models of secondary-ion emission.[1–5]

In contrast, the production of low-energy O^+ is wholly unrelated to elastic processes. Instead, it appears to be related to electronic energy deposition, since at velocities $<2\times10^8$ cm/sec (as is the case for the heavier beams), S_e is proportional to projectile velocity. Since total secondary-electron yields are known to be approximately proportional to electronic stopping powers (see Ref. 18 for a recent review of the subject), we hypothesize that these ions are emitted as a result of electronic transitions induced by secondary electrons which are produced as a result of ion bombardment. Electron stimulated desorption (ESD) of O^+ from vanadium oxide generally shows a threshold at an electron energy of approximately 30 eV.[19] Although secondary-electron energy distributions are peaked far lower than that ($\sim$2 eV), there is an increasingly significant contribution from higher-energy electrons as the ion beam energy is increased.[18] Furthermore, studies involving a variety of elemental polycrystalline surfaces have shown that in the range of the beam energies and species (both light and heavy) of interest, secondary electron yields vary slowly as a function of Z_1 and have incident beam velocity dependences similar to those which we have observed for the low-energy O^+ secondary-ion yields.[20–22]

It is also likely that specific Auger electrons produced in the decay of core-holes created as a result of ion bombardment are involved in this desorption, as has been suggested by Williams in his work on F^+ yields from flourinated Si.[6] He found that unlike the O^+ yields reported here, the yield of F^+ produced by (2–10)-keV Ar^+ bombardment increased much more rapidly than electronic

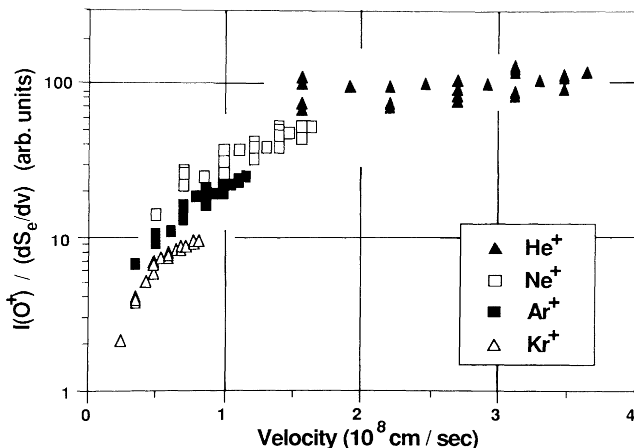

FIG. 8. The ratio $I(O^+)/(dS_e/dv)$ as a function of primary ion velocity, where $I(O^+)$ is the measured intensity of O^+ secondary ions and dS_e/dv is the low-velocity constant of proportionality between electronic stopping and primary-ion velocity calculated as in Ref. 23.

stopping power or, equivalently, total secondary electron yields. Since he was working in an energy regime just above the predicted threshold for production of these core holes, such a rapid rise would be expected. For the results reported here, however, the larger electronic excitation produced by the primary beam and the observed velocity proportionality of the O^+ yields, make it likely that true secondary electrons (that is, multiply scattered electrons which have lost some or all memory of their origin) are responsible for the majority of the O^+ emission.

There is one additional aspect of these data which requires comment. This is the remarkable similarity of the O^+ yield data for Ne, Ar, and Kr bombardment shown in Fig. 7. There is general agreement that the electronic stopping power of these ions is proportional to primary ion velocity v at the energies under consideration here.[23] However, the theoretical constant of proportionality is significantly different for each case. Thus, it was quite surprising to find that linear regression performed separately on the data for each primary ion yielded results that agreed (within the estimated errors) both in slope and intercept. That is, the data for Ne, Ar, and Kr bombardment lie *on a single line* when plotted as a function of v. It had been our expectation that when the O^+ yield data for each Z_1 were normalized to the low velocity value of dS_e/dv, which should be a constant for each ion, that the data of Fig. 7 would define a universal curve as a function of v. As is shown in Fig. 8, this did result in a more orderly placement of the He data. However, the colinearity of the other data points was broken. Clearly more experimental work is indicated to determine whether or not this feature of the data is accidental or whether it is common to other systems which emit O^+ copiously under fast ion bombardment.

A number of additional experiments are suggested by the more general hypothesis that O^+ production is related to high-energy secondary electrons. Among the most important of these is to determine the systematic behavior of the secondary electron spectrum as a function of incident beam energy, with special emphasis placed on electrons whose energies exceed ~30 eV. Such measurements are currently under way in our laboratory. In addition, comparisons of the energy distributions of O^+ ions produced by conventional ESD and ion bombardment as described here would be quite important.

V. CONCLUSIONS

We have shown that the yields of positive metallic and oxygen ions from clean and oxidized vanadium surfaces under bombardment by a wide range of ion species from (25—275)-keV are unrelated. Metallic ion yields are proportional to the sputtering yield of pure V as a function of both projectile species and energy. In contrast, the yield of O^+ increases linearly with projectile velocity in a manner similar to the electronic stopping power or, equivalently, the total secondary-electron yield. Hence, while the production of metallic ions may be described by a number of the proposed mechanisms of secondary-ion emission, that of O^+ cannot. We propose that the O^+ secondary ions originate from true ESD events initiated by secondary electrons produced by the incident beam.

ACKNOWLEDGMENTS

This work has been supported in part by U.S. Department of Energy under Contract No. DE-AC02-76ER03074 and a Cottrell Research Grant from the Research Corporation. The authors are very much indebted to M. R. Weller, L. M. Baumel, K. M. Hubbard, M. G. Kaurin, and J. P. O'Connor for their valuable assistance and discussions. We would also like to thank D. A. Bromley for his encouragement and support.

[1]K. Wittmaack, in *Inelastic Ion-Surface Collisions,* edited by N. H. Tolk, J. C. Tully, W. Heiland, and C. W. White (Academic, New York, 1977), p. 153.

[2]G. Blaise and A. Nourtier, Surf. Sci. **90**, 495 (1979).

[3]P. Williams, Surf. Sci. **90**, 588 (1979).

[4]G. Slodzian, Phys. Scr. **T6**, 54 (1983).

[5]M. L. Yu and N. D. Lang, Nucl. Instrum. Methods B **14**, 403 (1986).

[6]P. Williams, Phys. Rev. B **23**, 6187 (1981).

[7]J. P. O'Connor, P. G. Blauner, and R. A. Weller, Nucl. Instrum. Methods B **7/8**, 768 (1985).

[8]P. G. Blauner, J. P. O'Connor, and R. A. Weller, Nucl. Instrum. Methods B **12**, 343 (1985).

[9]J. P. O'Connor, P. G. Blauner, and R. A. Weller, Nucl. Instrum. Methods B **13**, 338 (1986).

[10]O. Becker, W. Knippelberg, and K. Wien, Phys. Scr. **T6**, 117 (1983).

[11]P. G. Blauner, M. R. Weller, M. G. Kaurin, and R. A. Weller,

Nucl. Instrum. Methods B **13**, 369 (1986).

[12]P. G. Blauner and R. A. Weller, following paper, Phys. Rev. B **35**, 1492 (1985).

[13]N. Matsunami *et al.*, At. Data Nucl. Data Tables **31**, 1 (1984).

[14]P. H. Dawson, in *Quadrupole Mass Spectrometry and Its Applications,* edited by P. H. Dawson (Elsevier Scientific, New York, 1976), p. 9.

[15]*UTI100c Operation and Service Manual* (Uthe Technology International, Sunnyvale, California, 1979).

[16]R. F. Garrett and R. J. MacDonald, Nucl. Instrum. Methods **191**, 308 (1981).

[17]A. Müller and A. Benninghoven, Surf. Sci. **39**, 427 (1973).

[18]N. Benazeth, Nucl. Instrum. Methods **194**, 405 (1982).

[19]M. L. Knotek and P. J. Feibelman, Phys. Rev. Lett. **40**, 964 (1978).

[20]G. Holmén, B. Svensson, and A. Burén, Nucl. Instrum. Methods **185**, 523 (1981).

[21]B. Svensson and G. Holmén, J. Appl. Phys. **52**, 6928 (1981).

[22]D. Hasselkamp, K. G. Lang, A. Scharmann, and N. Stiller, Nucl. Instrum. Methods **180**, 349 (1981).

[23]J. Lindhard, M. Scharff, and H. E. Schiøtt, Mat. Fys. Medd. Dan. Vid. Selsk. **33**, 1 (1963).

[24]P. Sigmund, Phys. Rev. **184**, 383 (1969).